Mon. Not. R. Astron. Soc. **000**, 000–000 (0000) Printed 21 November 2012 (MN LATEX style file v2.2)

The baryonic properties of the Local Group: a semi-analytic perspective

Sergio Sanes ⋆[1], Jaime E. Forero-Romero[2], Juan C. Munoz-Cuartas[2], Luis F. Quiroga-Pelaez[1], Jorge I. Zuluaga[1], Stefan Gottlöber[2], Yehuda Hoffman[3], Gustavo Yepes[4]

[1] *Universidad de Antioquia*
[2] *Leibniz-Institut für Astrophysik Potsdam (AIP), An der Sternwarte 16, 14482 Potsdam, Germany*
[3] *Racah Institute of Physics, Hebrew University, Jerusalem 91904, Israel*
[4] *Grupo de Astrofísica, Universidad Autónoma de Madrid, Madrid E-28049, Spain*

21 November 2012

ABSTRACT

Key words: galaxies: evolution - galaxies: formation - galaxies: high-redshift - methods: N-body simulations

1 INTRODUCTION

2 SEMI-ANALYTICS AND THE SIMULATIONS

2.1 The Semi-Analytic Method

We use the semi-analytic code of galaxy formation Galacticus (Benson 2010), designed to by means of the hierarchical merging history of a dark matter halo, estimate the properties of the galaxies hosted in it at any instant of its evolution.

The code can include any model of physical process, starting from the generation of random dark matter density distributions to calculate stellar population properties while implementing accretion of gas, cooling, stellar and supernovae feedback. Depending of the needs, it is capable of generate its own Monte Carlo merger trees or just read merger trees provided by cosmological simulations as we did taking advantage of the CLUES[1] project[2] simulations. The remaining of this section is dedicated to explain how Galacticus model the key astrophysical processes regarding our research.

Halos can increase their mass a consequence of mergers or accretion from the interstellar medium. In our selected model the accretion rate of gas from the interstellar medium into a dark matter halo is modeled by assuming that the amount of accreted baryonic matter is directly related to the amount of accreted dark mass by the universal baryonic fraction Ω_b/Ω_M. This can be expressed as

$$\dot{M}_{\rm accre} = \begin{cases} (\Omega_b/\Omega_M)\dot{M}_{\rm halo}, & \text{if} \quad V_{\rm virial} > V_{\rm reioniz} \\ & \text{or} \quad z > z_{\rm reioniz} \\ 0, \text{otherwise} & \end{cases} \tag{1}$$

where the effects of reionization are taken in to account by imposing the condition that no gas can be accreted at redshifts z higher than the one of reionization $z_{\rm reioniz}$ or if the virial velocity $V_{\rm virial}$ is less than the one of reionization $V_{\rm reioniz}$. In case of a merger the whole mass of the satellite $M_{\rm satel}$ and central $M_{\rm central}$ goes to the bulge component of the central galaxy when the satellite-to-central mass ratio $M_{\rm central}/M_{\rm satel}$ is above the major-to-minor merger fraction η, meaning a major merger. If a minor merger occurs the mass of the central galaxy does not moves, the stars of the satellite goes to the bulge of the central and according to a a free parameter of the model the gas mass $M_{\rm satel.,gas}$ can be moved to the disk or to the bulge.

The cooling rate according to White & Frenk (1991) is given by

$$\dot{M}_{cool} = 4\pi r_{\rm cool}^2 \rho(r_{\rm cool}) \dot{r}_{\rm cool} \tag{2}$$

where $\rho(r)$ is the density profile of the hot halo and the cooling raduis $\dot{r}_{\rm cool}$ is calculted by seeking the radius at which the time available for cooling equals the cooling time $t_{\rm cool}$.

Then the cooled gas is transformed into stars according to the star formation rate of the spheroid and disk components of the galaxy which are assumed to be fixed and of the form $\phi = M_{\rm gas}/\tau_\star$, where $M_{\rm gas}$ is the amount cold gas and

$$\tau_\star = \epsilon_\star^{-1} \tau_{\rm dyn} \left(\frac{V}{200 {\rm km/s}} \right)^{\alpha_\star} \tag{3}$$

⋆ email
[1] Constrained Local UniversE Simulations
[2] `http://www.clues-project.org/`

is the star formation time scale (a similar expression of the one of Baugh et al. (2005)) where $\tau_{\rm dyn}$ is the dynamical time defined as $\tau_{\rm dyn} = R_{\rm virial}/V_{\rm circ}$, $R_{\rm virial}$ and $V_{\rm circ}$ are the characteristic radius and velocity respectively, the free parameter $\epsilon_\star$ is the star formation efficiency and $\alpha_\star$ is a free parameter as well.

We used the simplest method to model the increase of stellar mass. We relate the star formation rate ϕ to the stellar mass rate $\dot{M}_\star$ by a means of a constant rate of decrease of fuel mass as

$$\dot{M}_\star = (1-R)\phi, \tag{4}$$

where R is the instantaneous recycled fraction. The rate of the metal content of the fuel changes as the star formation rate, the yield p and R according to

$$\dot{M}_{{\rm fuel},Z} = -(1-R)Z_{\rm fuel}\phi + p\phi, \tag{5}$$

while the rate of change the metal content of the stars $\dot{M}_{\star,Z}$ follows from the fuel metallicity $Z_{\rm fuel}$. We have used the Salpeter initial mass function (Salpeter 1955) to estimate the values of R and p. Another important process we have aboarded is the supernovae feedback driven outflow that is modeled for the disks and the bulge of the galaxies through a power law relation and it is assumed to be proportional to the rate of energy pumped in to the gas by the stellar populations. The rate of change of the mass expulsed by supernovae is given by

$$\dot{M}_{\rm outflow} = \left(\frac{V_{\rm outflow}}{V}\right)^{\alpha_{\rm outflow}} \frac{\dot{E}}{E_{\rm canonical}}, \tag{6}$$

where $V_{\rm outflow}$ is the velocity of the ejected outflow mass due to supernovae, V is the characteristic velocity, $\dot{E}$ is the rate of change of the energy transmitted to the gas by stars and $E_{\rm canonical}$ is the total energy transmitted by a stellar population normalized to $1M_\odot$.

2.2 Contrained N-body simulations and Merger Trees

In this section we briefly describe the information of the CLUES simulations relevant to our research, the procedure of constraining cosmological simulations and construction of merger trees.

We have selected the three available realizations for the WMAP5 cosmology of the CLUES (Gottloeber et al. 2010) which is aimed to provide constrained cosmological simulations recreating the Local Universe. As the CLUES simulations are intended to recreate the Local Universe they contain a set of dark matter halos candidates that should host galaxies with properties quite similar to those of the ones of the Local neighborhood galaxies including the Milky Way and Andromeda. We will give special attention to those halos candidates that should contain the Milky Way and Andromeda which from now we will call a Local Group candidates. Each of these simulations includes 1024^3 particles with a mass of $m_p = 1.89 \times 10^7 h^{-1}{\rm M}_\odot$inside a box of side length $64h^{-1}$Mpc that provides an amount of more than 5×10^4 dark matter merger trees (Forero-Romero et al. 2011). The cosmological parameters are consistent with the WMAP5 cosmology in Komatsu et al. (2009) with a density $\Omega_m = 0.279$, a cosmological constant $\Omega_\Lambda = 0.721$, a dimensionless Hubble parameter $h = 0.70$, a spectral index of primordial density perturbations $n = 0.96$, a normalization $\sigma_8 = 0.817$. The code used to perform the simulations is the Tree-PM MPI N-body code Gadget2 (Springel 2005). From the set of three realizations for the WMAP5 cosmology we selected the set of merger trees whose dark matter halos at $z = 0$ are in the mass range $11.0 < \log_{10} M_{vir}/M_\odot < 13.0$ and make an special emphasys in the subrange $11.5 < \log_{10} M_{vir}/M_\odot < 12.5$ to study MW and M31-type galaxies.

The standard procedure of building by means of simulations a Local Universe able to recreate the main features of the observed is to constrain the initial conditions to observations. For the CLUES simulations it was used the Hoffman & Ribak (1991) algorithm to constrain the Gaussian random fields to observational data. Due to its very small changes in time, the velocity field played a crucial roll in constraining the initial conditions. To set up the velocity constrains the MARK III (Willick et al. 1997), SBF (Tonry et al. 2001) and the Karachentsev (Karachentsev et al. 2004) catalogs were used (Forero-Romero et al. 2011), for more details of the constraining procedure go to Gottloeber et al. (2010). As the constrains can only affect the large and meso scales, it was necessary to perform a large amount of low resolution simulations. Only three of all the simulations were had success in recreating under a certain accurately the properties of the dark matter distribution.

The catalogue of dark matter halo merger trees used is the one of Forero-Romero et al. (2011). To identify halos it was used a FOF (Friends-of-Friends) algorithm in 80 snapshots corresponding to an interval of about 13Grys between $0 < z < 7$, where it was not included any substructure information. It was used a linking length of $b = 0.17$ times the mean inter particle separation and the minimum resolved halo masses are of $M_{\rm min} = 3.78 \times 10^8 h^{-1}{\rm M}_\odot$. The procedure used to build the merger trees is the standard. Starting from the snapshot at $z = 0$, the particles bind to a particular halo of the catalogue are scanned in the first snapshot $z > 0$ and if there it is found any halo with more than thirteen particles then then this halo is called to be a progenitor of the former. The process is repeated over the whole catalogue at $z = 0$ and continued until the highest z. For more details about the halo identification and merger tree construction go to Forero-Romero et al. (2011).

To perform our simulations, it was only used the information relating the masses of the satellites and central dark matter halos over the different snapshots to its progenitors, the detailed information of how are built the input dark matter halo merger trees for Galacticus go to Benson (2010).

3 THE OBSERVATIONAL PRORPERTIES OF MW AND M31

In this section we present the values for the parameters we have chosen to define the MW and M31: disk stellar mass, disk gaseous mass and bulge stellar mass.

Disk stellar mass. The principal approach to estimate the stellar mass in the disk of our galaxy is dynamical modelling. The work of Klypin et al. (2002) uses a parametric model that does not distinguish between the cold (gas) component and the stars, their results for galaxy models that allow for exchange of angular momentum locate the total

baryonic mass of the disk between $5-6\times10^{10}$M$_\odot$for the MW and $7-9\times10$M$_\odot$for M31. Later Widrow & Dubinski (2005) use N-body realizations of self-consisten, equilibrium distributions of the dark matter and stellar compoents to address the same problem. Their models fit with good match to the observational data have stellar masses of $3.3-4.5\times10^{10}$M$_\odot$for the Milky Way and $7-10\times10^{10}$ for andromeda. (Geehan et al. 2006a) modeled the Andromeda strem using analytic bulge-disc-halo for M31, finding the best agreement for a disk mass of 8.4×10^{10}M$_\odot$. In this work we take $3.3-4.5\times10^{10}$M$_\odot$for the Milky Way and $7-10\times10^{10}$ for M31.

Bulge stellar mass. Klypin et al. (2002) constrain the MW bulge stellar masss $1-1.2\times10^{10}$ M$_\odot$while for M31 $1.9-2.4\times10^{10}$, for the same galaxy (Geehan et al. 2006a) find a bulge mass of 3.3×10^{10}M$_\odot$. The MW analytical model of model (Dehnen & Binney 1998) finds a range of different values with average $\sim0.510^{10}$M$_\odot$. In this work we pick $0.5-1.2\times10^{10}$M$_\odot$for the MW and $1.9-3.3\times10^{10}$M$_\odot$for M31.

Disk Gaseous mass. The abundance of gas in the Milky Way has been constrained through chemical evolution models. The set of observational constraints on these models most notably include the gas and star formation rate (SFR) profiles. The relevant observational data was compiled in (Boissier & Prantzos 1999) using from the original work in Kulkarni & Heiles (1987); Dame (1993), with a values of $6.0-8.0\times10^{9}$M$_\odot$, an update implementation of this chemical evolution model by (Yin et al. 2009a) uses the same observations. In the case of M31 the best observational constraints come from the observations by (Cram et al. 1980) with the integrated mass of neutral gas corrected by (Dame 1993), yielding a value of 5.2×10^{9}M$_\odot$, there is a systematic observational uncertainty of 5% originally quoted in (Cram et al. 1980), but due to oppacity effects of the HI (Braun & Walterbos 1992) the total value of gas can increase by a 19%. Therefore we keep a value of $5.0-6.0\times10^{9}$ for the mass of gas in the M31 disk and $6.0-8.0\times10^{9}$M$_\odot$for the Milky Way.

4 THE METHOD

4.1 Numerical Procedures

To achieve our goals we have used the semi-analytic code Galacticus v0.0.1 to perform semi-analytical simulations of different models to study the $z=0$ properties of the simulated galaxies. The amount of halos in our selected mass range in section 2.2) is above 9000/box, then, accounting for a total of almost 30000 merger trees when the three boxes are included. In this section we investigate how sensitive could be the properties of the simulated galaxies to the variations of several parameters we pretent to study. To do this, we have simulated a set of models with parameters as shown Table 1 where to be in agreement to the data we have settled the respective cosmology to WMAP5 and any other not mentioned parameters are settled to the code's default values (To see in detail the parameters and their values go to Benson (2010)). From the simulated models of Table 1 we have defined three benchmarks, the first is R1 which is performed with a spin parameter distribution according to the one of Bett et al. (2007). For he two other simulated models R2 and R3, we have settled the distribution of the spin parameter to a Lognormal distribution with a mean $\mu_\lambda=0.03687$ and dispersion $\sigma_\lambda=0.2216$ according to the work of Muñoz-Cuartas et al. (2011) but in R2 the gas of satellites after a minor merger goes to the bulge of the central galaxy and in the R3 the gas goes to the disk of the central galaxy. All the remaining models are settled to a Lognormal distribution with a mean $\mu_\lambda=0.03687$ and dispersion $\sigma_\lambda=0.2216$ as well. We have developed a set of four experiments intended to study how are affected the stellar-to-dark matter ratio, gas-to-total mass ratio and bulge-to-total mass ratio by the variation of $\alpha_{\rm outflow}$, $\epsilon_\star$ for the disk component of the galaxies, η and where does $M_{\rm satel.,gas}$ goes after a minor merger.

As discribed in Table 1, in the set of E-labeled models, from our the selected halo population we have modeled galaxies with $\epsilon_{disk,\star}=0.01,0.02,0.035,0.05,0.075$ and 0.1; In the A-labeled models, we selected the four values 1.5, 2.0, 2.5 and 3.0 for the $\alpha_{\rm disk,outflow}$ parameter; In the D and B-labeled models we performed simulations to search wether there is any correlation between the studyed properties and the parameter $M_{\rm satel.,gas}\rightarrow$ when it is settled to the disk and to the bulge, so, as we have a special interested in obtaining disk-type galaxies, for the most of the models of Table 1 we have settled $M_{\rm satel.,gas}\rightarrow$ to the disk. In the two other experimets we set $M_{\rm satel.,gas}\rightarrow$ to the disk and bulge while η is settled to 0.2,0.3 and 0.4.

4.2 Searching LG-type Galaxies

Our investigation of the LG can be divided into two main parts. The first is intended to study for the different models in Table 1, the formation of MW and M31-type galaxies given a catalogue of dark matter merger trees; In the second one, we study how peculiar are the LG candidates provided from the CLUES simulations in terms of the similarity of their properties compared to the observed ones.

To study the similarity between the observed and the simulated galaxy we make use of relative errors. Let an observed galaxy $\rho_{obs}(p_{obs,1},\ldots,p_{obs,n})$ be characterized by an amount of n observed properties $p_{obs,i}$, a simulated galaxy $R_{sim}(r_{sim,1},\ldots,r_{sim,n})$ characterized by the same amount of estimated properties $r_{sim,i}$. The relative error between each observated property and the modelled is $\epsilon_i=|P_{obs,i}-R_{sim,i}|/|P_{obs,i}|$. Then, we would use the addition of all the relative errors of all the properties

$$\Delta\varepsilon=\epsilon_i+\cdots+\epsilon_n. \quad (7)$$

To study how much changes the abundance of LG-type galaxies for each of the performed models, we accounted the amount of galaxies $N(\Delta\varepsilon)$ similar to the MW and M31 under a ranges of calculated total relative error $\Delta\varepsilon$ as defined in equation 7. We selected three the lowest values of $\Delta\varepsilon$ (0.08, 0.16 and 0.24) and studyed its variations of $N(\Delta\varepsilon)$ as a function of the studyed parameters in order find lights about wether there is any set values for our selected set of parameter that 1) increases the abundace of disk galaxies 2) increases the amount of MW and M31-type of galaxies.

Model	$z_{reioniz}$	$M_{\rm satel.,gas} \rightarrow$	η	$P(\lambda)$	μ_λ	σ_λ	$\alpha_{\rm disk,outflow}$	$\epsilon_{\rm disk,\star}$
R1	9.0	bulge	0.3	Bett 2007			2.0	0.01
R2	7.0	bulge	0.3	Lognormal	0.031	0.57	2.0	0.01
R3	7.0	disk	0.3	Lognormal	0.031	0.57	2.0	0.01
E1	7.0	disk	0.3	Lognormal	0.031	0.57	2.0	0.02
E2	7.0	disk	0.3	Lognormal	0.031	0.57	2.0	0.035
E3	7.0	disk	0.3	Lognormal	0.031	0.57	2.0	0.05
E4	7.0	disk	0.3	Lognormal	0.031	0.57	2.0	0.075
E5	7.0	disk	0.3	Lognormal	0.031	0.57	2.0	0.1
A1	7.0	disk	0.3	Lognormal	0.031	0.57	1.5	0.01
A2	7.0	disk	0.3	Lognormal	0.031	0.57	2.5	0.01
A3	7.0	disk	0.3	Lognormal	0.031	0.57	3.0	0.01
D1	7.0	disk	0.2	Lognormal	0.031	0.57	2.0	0.01
D2	7.0	disk	0.4	Lognormal	0.031	0.57	2.0	0.01
B1	7.0	bulge	0.2	Lognormal	0.031	0.57	2.0	0.01
B2	7.0	bulge	0.4	Lognormal	0.031	0.57	2.0	0.01

Table 1. Set of four experiments intended to model the galaxies hosted in halos of mass range of $11.0 < log_{10} M_{\rm DM} < 13.0$.

Property	MW	Ref.	M31	Ref.
$M_{disk,\star}[10^{10} M_\odot]$	3.0	(1)	7.2	(2)
$M_{disk,gas}[10^{10} M_\odot]$	0.7	(3)	0.6	(4)
$M_{bulge,\star}[10^{10} M_\odot]$	$1-2$	(3)	3.2	(2)
V_{circ}[Km/s]	238	(5)	275 ± 5	(6)

Table 2. Observational estimations for different properties of the LG, where(1)Zheng et al. (2001), (2) Geehan et al. (2006b), (3)Yin et al. (2009b), (4) Nieten et al. (2006), (5)Battaglia et al. (2005), (6)Seigar et al. (2008).

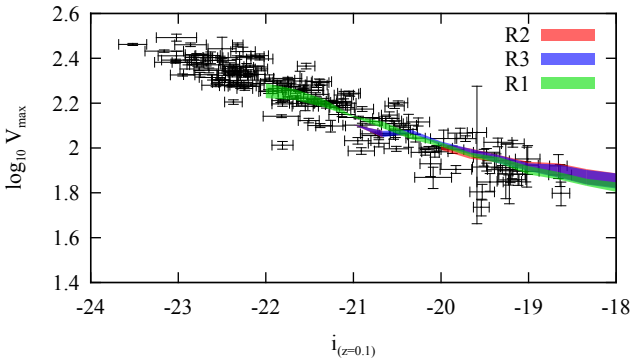

Figure 1. Tully fischer relation. The magnitudes where calculated without dust extintion and the parameters of the models can be seen at Table 1 as R1, R2 and R3. The error bars correspond to the results of Pizagno et al. (2007).

4.3 Modeling the LG candidates

We proceded to model semi-analyticaly the pairs of LG candidates available from the three WMAP5 boxes of CLUES.

Two experiments were performed. Given the preliminar results of sections 4.1 and 4.2, we settled the space parameter of the two experiments to a WMAP5 cosmology and $M_{\rm satel.,gas} \rightarrow$ to the disk component of the galaxy. The first experiment was intended to recreate the experiment of the A-labeled models of Table 1, so, we simulated the LG halo candidates for different values of $\alpha_{\rm disk,outflow}$ ranging from 1.5 to 3.0 in steps of 0.075. For each of the values of $\alpha_{\rm disk,outflow}$, we repeated the simulation 100 times and calculated the medians of the properties of MW and M31; In the second experiment, we recreate the experiement of the E-labeled models. We simulated the LG candidates through 20 different models of $\epsilon_{\rm disk,\star}$, starting from 0.005 in steps of 0.005 to 0.1, repeated the simulation 100 times for each value of $\epsilon_{\rm disk,\star}$ and calculated the medians of the properties as well. Finally it was also applied the same searching criterium of equation 7 to look for similarities between the LG modeled pairs and the observed M31 and MW.

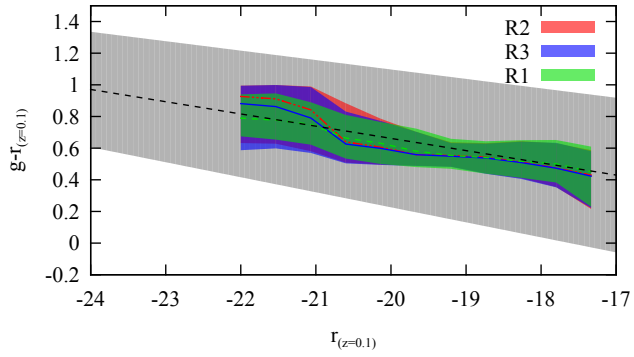

Figure 2. Color magnitud relation. Magnitudes were calculated without extintion. This is the reference simulation presented in table 1 as R1, R2 and R3. The shaded region correspond to a scatter of 2σ from the work of Muñoz-Cuartas & Müller (2012).

5 RESULTS

5.1 Test on Galacticus

We calculated the Tully-Fisher and Color-Magnitude relations for each of the models in Table 1. To build the Tully-Fisher relation, we proceded selecting the maximum velocity between the bulge and disk components of disk galaxies, and defined disks as galaxies with a bulge-to-total mass ratio $M_{\rm bulge}/M_{\rm tot} \leq 0.3$.

In Figure 1 are shown de scatters of the maximum velocity between the first and thirth quartils as a function of magnitude in the i-band without dust extintion of the data of the three benchmarks R1, R2 and R3 compared to the data of the SDSS (Pizagno et al. 2007). It can be seen the resulting Tully-Fisher relations of each of the benchmarks reproduce accurately the one of the SDSS. In general none of the calculated Tully-Fisher relations of any of the simulated models deviate significantly from ones shown in 1. We have also calculated the Color-Magnitude diagrams without dust extintion of the three mentioned benchmarks. In Figure 2, the scatter of the color between the first and thirth quartils and the medians as a function of the r-band reproduce accurately the estimated Color-Magnitude relation of the SDSS (Muñoz-Cuartas & Müller 2012). Again, in general, all the other simulated models of the calculated medians does not deviate significantly from the estimations of the best fit of the mean of the SDSS and remains inside of the 3σ estimated deviation of the Color-Magnitude relation.

Besides, as we stated in Section 4.1, we developed four experiments intended to study the changes in the stellar-to-dark matter ratio, gas-to-total mass ratio and bulge-to-total mass ratio of the simulated galaxies according to the variation in the different models of $\alpha_{\rm outflow}$, $\epsilon_\star$, η and $M_{\rm satel.,gas} \rightarrow$, as described in Table 1.

In Figure 3 are presented the results of three of the above mentioned experiments. The three panels of the left row show the results of the modification of the supernovae activity through four different values of $\alpha_{\rm outflow}$ in the disk component of the simulated galaxies, the A-labeled models of Table 1; The three panels of the central row correspond to the E-labeled models, where we modeled our halo population for six different values of $\epsilon_{\rm disk,\star}$; And, in the three right panels are the results of the D-labeled models, where it is modified the value of the η parameter when $M_{\rm satel.,gas} \rightarrow$ is settled to the disk component.

The panels on top of Figure 3 show the calculated medians of the stellar-to-dark matter ratio relations of each of the experiments, the central panels are the medians of the gas-to-total mass ratio as a funcion of the stellar mass and the ones at the bottom are medians of the bulge-to-total mass ratio as a function of the stellar mass. In the plot at the left on top, galaxies with a total stellar mass content below $3.2 \times 10^{10} M_\odot$ shows a decrease in the amount of the stellar content as it is increased the rate of ejected mass by supernovae, and then, as it is expected, the amount of gas content is increased as can be seen at the left central plot. The morphology of the galaxies is affected as well. Shown at the bottom left panel of Figure 3, the net effect of increasing the $\alpha_{\rm disk,\ outflow}$ parameter produces a decrease of the bulge-to-total mass ratio, so, it increases the amount of disk galaxies. Nevertheless the four values of the $\alpha_{\rm disk,\ outflow}$ parameter keep the the gas-to-total mass ratio relations under good agreement with observations and the bulge-to-total mass ratio relations behaves as it is espected, only the values between 2.5 and 3.0 are the ones that can enclose the stellar-to-halo mass relation. 2.5 and 3.0 are respectively upper and lower limits of $\alpha_{\rm disk,\ outflow}$ for the stellar-to-halo mass relation of Moster et al. (2010).

In the top central panel of Figure 3, the stellar-to-halo mass relation show a trend related to the star formation in the disk component of galaxies. As $\epsilon_{\rm disk,\star}$ increases the faint end of the stellar-to-halo mass relation tend to decrease while the bright end increases. It has to be remarked that while the stellar-to-halo mass relation changes, the calculated medians of the relation for the six different models remain almost fixed arround the peak of the relation at $1 \times 10^{12} M_\odot$. In the central panel, a low star formation rate in galaxies with a stellar mass lower than $3.2 \times 10^{10} M_\odot$ increase the gas-to-total mass ratio. In the central bottom panel we can see the increase of the $\epsilon_{\rm disk,\star}$ clearly modifies the morphology of galaxies. A higher $\epsilon_{\rm disk,\star}$ increases the disk component masses of the whole population of simulated galaxies and then the abundace of disk galaxies is increased. Nevertheless the gas-to-total mass ratio relation keeps inside the observations for the different E-labeled models when is compared to the data provided in Bell et al. (2003b) and Bell et al. (2003a), the highest values of $\epsilon_{\rm disk,\star}$ are the ones that provide a relation closer to the one of Moster et al. (2010). The three right panels of Figure 3 show the results of the D-labeled models where it has been settled $M_{\rm satel.,gas} \rightarrow$ to the disk component and simulated for different values of η. It was not found any correlation between the η parameter and the calculated properties, not even when $M_{\rm satel.,gas} \rightarrow$ was settled to the bulge in the B-labeled models.

5.2 Abundance of M31 and MW-type galaxies

Now, we will analyse how changes the abundance of LG-type galaxies for the group of experiments defined in Table 1. To do that, we selected halos with a $z = 0$ virial mass between $11.5 < \log_{10} M_{\rm DM}/M_\odot < 12.5$; calculated $N(\Delta\varepsilon)$ in ranges of $\Delta\varepsilon$ for the observed properties of the MW and M31 in Table 2; and, study the $N(\Delta\varepsilon)$ of the lowest values of $\Delta\varepsilon$ as a function of function of $\alpha_{outflow}$, $\epsilon_\star$, η for the different models.

In Figure 5 are plotted the $N(\Delta\varepsilon)$ of the three lowest values of $\Delta\varepsilon$ for MW and M31-type galaxies as a function of $\alpha_{\rm outflow}$ calculated for the set of A-labeled models of Table 1, where the value of $\alpha_{\rm outflow}$ was increased from 1.5 in steps of 0.5 to 3.0. It can be observed that higher values of $\alpha_{\rm outflow}$ increases the amount of LG-type galaxies but priviledges the increase of the abundace of MW-type galaxies more than that of M31-type galaxies.

Nevertheless an increase of the value of $\alpha_{\rm outflow}$ would produce a higher amount of LG-type galaxies, the overstate of the supernovae feedback activity produces a decrease of the stellar-to-halo mass relation for halos with $M_{\rm DM} \leq 1 \times 10^{12} M_\odot$ as can be seen at the plot at the left on top of the Figure 3. We found that under the space parameter configuration of the simulated A-labeled models, the proper values of $\alpha_{\rm outflow}$ for modeling the supernovae feedback through equation 6 can only be between $2.5 \lessapprox \alpha_{\rm outflow} \lessapprox 3.0$, and, to increase the abundance of disk

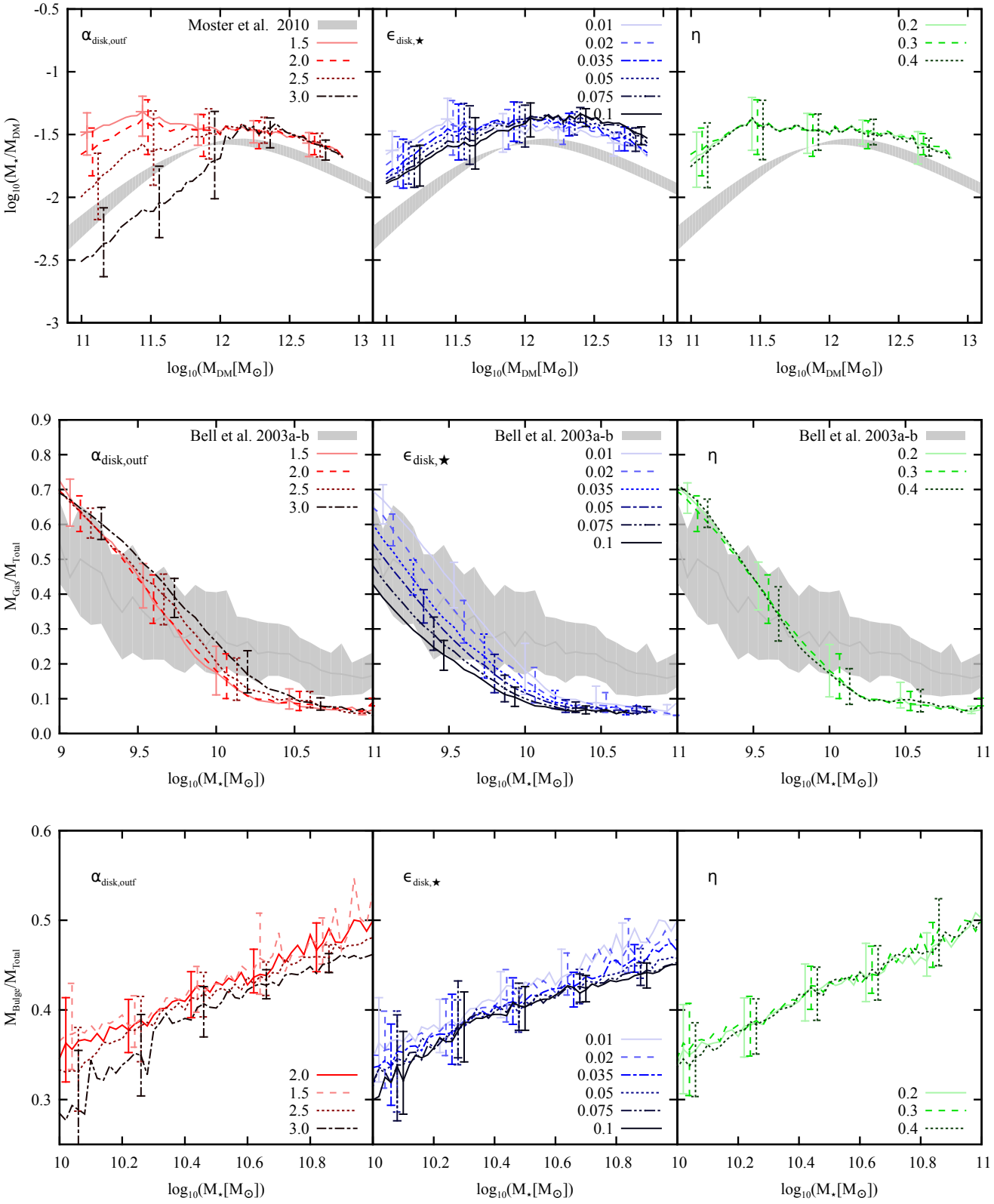

Figure 3. Top: Calculated medians of the stellar-to-halo mass relation compared against the relation of Moster et al. (2010) between the first and thirdth quartils. Central: Medians of the gas-to-total mass fraction as a function of the stellar mass compared to Bell et al. (2003b) and Bell et al. (2003a) between the first and thirdth quartils. Bottom: Medians of the bulge-to-total mass fraction as a function of the stellar mass. The first row of the three plots correspond to the variation of the $\alpha_{\rm outflow}$, the second to the variation of $\epsilon_\star$ and the last to the variation of η when the gas of the satellite goes to the disk of the galaxy. The error bars of each line correspond to the range of the data between the first and thirdth quartils.

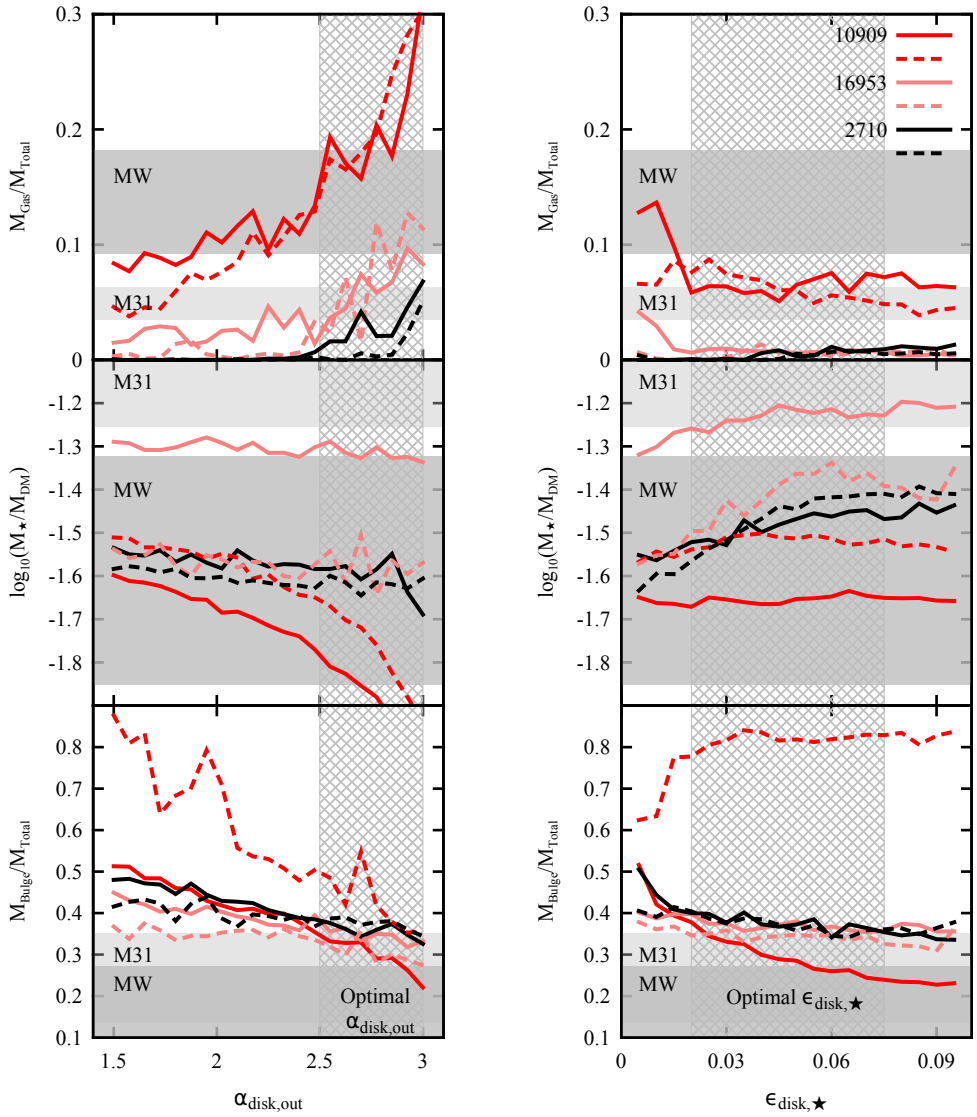

Figure 4. Estimated medians of the modeled properties for the MW and M31 as a function of $\epsilon_\star$ on the right and $\alpha_{\rm outflow}$ on the left. Top: Gas-to-total mass ratio. Central:Stellar mass-to-dark matter mass ratio relation. Bottom: Bulge-to-total mass ratio relation. Horizontal shaded regions correspond to the observational estimations of the MW and M31. The striped regions correspond to the values of the parameters that produce best agreement to the stellar-to-halo mass, gas-to-total mass relations and bulge fraction.

galaxies and then LG-type galaxies, should be choosen the highest values $\alpha_{\rm outflow}$ below 3.0.

We also made an analysis like the above with the $\epsilon_\star$ parameter for the E-labeled models. Figure 6 shows the values of $N(\Delta\varepsilon)$ for the three lowest values of $\Delta\varepsilon$ calculated for LG-type galaxies as a function of $\epsilon_\star$.

Even though higher values of $\epsilon_\star$ increases the abundace of disk galaxies, the increase of the star formation in the disk component of the sample of simulated galaxies does not favorate the formation of LG-type galaxies, on the contrary, the decrease of the parameter favorates it.

The performed D-labeled simulations with different values of η; intended to see wether this parameter affects the formation or LG-type galaxies or not, showed no correlation between η and $N(\Delta\varepsilon)$. As can be seen at the right plots of Figure 3, the shape of the simulated properties for our sample galaxies is not affected by the η parameter. Nevertheless of the previous result, we found that the redirection of the gas of a satellite after a minor merger to the disk instead of the bulge does favorate the searched situation, as it can be seen in Figure 7 where we compare $N(\Delta\varepsilon)$ of models R2 and R3 calculated for MW and M31-like galaxies.

5.3 The MW and M31 candidates

As described in section , to study the LG candidates of the CLUES WMAP5 simulations we runned 20 models where we repeated over 100 times the estimation the properties in each of the models and the calculated the medians of each property. In Figure 4 can be observed the estimated medians for the stellar mass, gas fraction and bulge fraction as a function of the parameters $\epsilon_\star$ and $\alpha_{\rm outflow}$. It can be observed

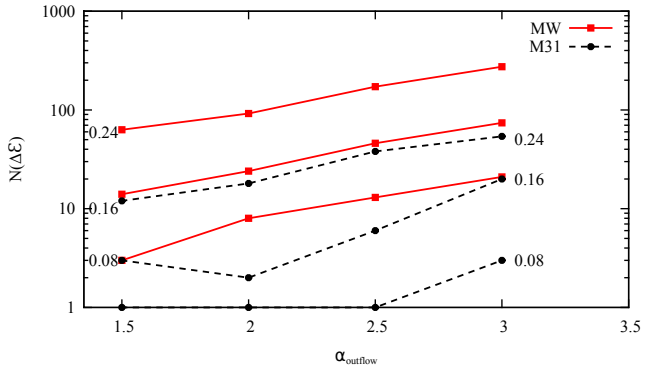

Figure 5. $N(\Delta\varepsilon)$ as a function of $\alpha_{\rm outflow}$. $N(\Delta\varepsilon)$ for the three lowest values of $\Delta\varepsilon = 0.08, 0.16, 0.24$ as a consecuense of the variation of $\alpha_{\rm outflow}$ parameter.

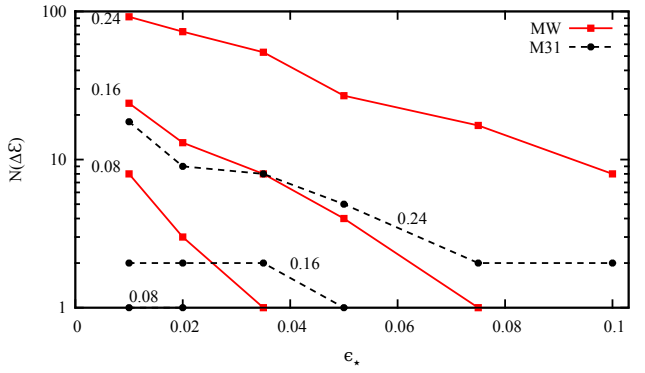

Figure 6. $N(\Delta\varepsilon)$ as a function of $\epsilon_\star$. $N(\Delta\varepsilon)$ for the three lowest values of $\Delta\varepsilon = 0.08, 0.16, 0.24$ as a consecuenseof the variation of $\epsilon_\star$ parameter.

that each pair of LG corresponding to the same simulations have a similar behavior as the values of the parameters are changed.

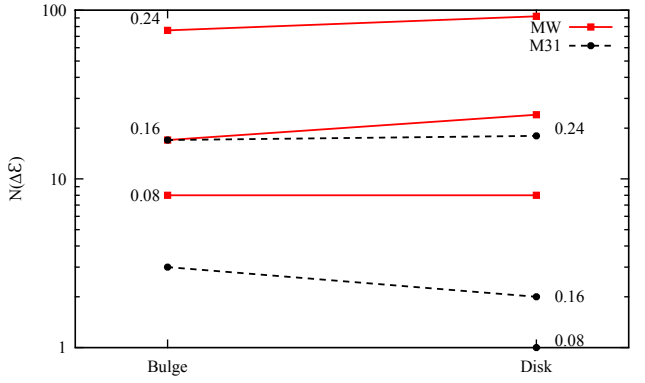

Figure 7. The values of $N(\Delta\varepsilon)$ for the three lowest values of $\Delta\varepsilon = 0.08, 0.16, 0.24$ when the gas of a satellite after a merger goes to the disk and to de bulge.

6 CONCLUSIONS AND DISCUSION

ACKNOWLEDGMENTS

REFERENCES

Battaglia G., Helmi A., Morrison H., Harding P., Olszewski E. W., Mateo M., Freeman K. C., Norris J., Shectman S. A., 2005, MNRAS, 364, 433

Baugh C. M., Lacey C. G., Frenk C. S., Granato G. L., Silva L., Bressan A., Benson A. J., Cole S., 2005, MNRAS, 356, 1191

Bell E. F., McIntosh D. H., Katz N., Weinberg M. D., 2003a, ApJL, 585, L117

Bell E. F., McIntosh D. H., Katz N., Weinberg M. D., 2003b, ApJS, 149, 289

Benson A. J., 2010, ArXiv e-prints

Bett P., Eke V., Frenk C. S., Jenkins A., Helly J., Navarro J., 2007, MNRAS, 376, 215

Boissier S., Prantzos N., 1999, MNRAS, 307, 857

Braun R., Walterbos R. A. M., 1992, ApJ, 386, 120

Cram T. R., Roberts M. S., Whitehurst R. N., 1980, A&AS, 40, 215

Dame T. M., 1993, in Holt S. S., Verter F., eds, Back to the Galaxy Vol. 278 of American Institute of Physics Conference Series, The distribution of neutral gas in the Milky Way. pp 267–278

Dehnen W., Binney J., 1998, MNRAS, 294, 429

Forero-Romero J. E., Hoffman Y., Yepes G., Gottoeber S., Piontek R., Klypin A., Steinmetz M., 2011, ArXiv e-prints

Geehan J. J., Fardal M. A., Babul A., Guhathakurta P., 2006a, MNRAS, 366, 996

Geehan J. J., Fardal M. A., Babul A., Guhathakurta P., 2006b, MNRAS, 366, 996

Gottloeber S., Hoffman Y., Yepes G., 2010, ArXiv e-prints

Hoffman Y., Ribak E., 1991, ApJL, 380, L5

Karachentsev I. D., Karachentseva V. E., Huchtmeier W. K., Makarov D. I., 2004, AJ, 127, 2031

Klypin A., Zhao H., Somerville R. S., 2002, ApJ, 573, 597

Komatsu E., Dunkley J., Nolta M. R., Bennett C. L., Gold B., Hinshaw G., Jarosik N., Larson D., Limon M., Page L., Spergel D. N., Halpern M., Hill R. S., Kogut A., Meyer S. S., Tucker G. S., Weiland J. L., Wollack E., Wright E. L., 2009, ApJS, 180, 330

Kulkarni S. R., Heiles C., 1987, in Hollenbach D. J., Thronson Jr. H. A., eds, Interstellar Processes Vol. 134 of Astrophysics and Space Science Library, The atomic component. pp 87–122

Moster B. P., Somerville R. S., Maulbetsch C., van den Bosch F. C., Macciò A. V., Naab T., Oser L., 2010, ApJ, 710, 903

Muñoz-Cuartas J. C., Macciò A. V., Gottlöber S., Dutton A. A., 2011, MNRAS, 411, 584

Muñoz-Cuartas J. C., Müller V., 2012, MNRAS, 423, 1583

Nieten C., Neininger N., Guélin M., Ungerechts H., Lucas R., Berkhuijsen E. M., Beck R., Wielebinski R., 2006, A&A, 453, 459

Pizagno J., Prada F., Weinberg D. H., Rix H.-W., Pogge R. W., Grebel E. K., Harbeck D., Blanton M., Brinkmann J., Gunn J. E., 2007, AJ, 134, 945

Salpeter E. E., 1955, ApJ, 121, 161

Seigar M. S., Barth A. J., Bullock J. S., 2008, MNRAS, 389, 1911

Springel V., 2005, MNRAS, 364, 1105
Tonry J. L., Dressler A., Blakeslee J. P., Ajhar E. A., Fletcher A. B., Luppino G. A., Metzger M. R., Moore C. B., 2001, ApJ, 546, 681
White S. D. M., Frenk C. S., 1991, ApJ, 379, 52
Widrow L. M., Dubinski J., 2005, ApJ, 631, 838
Willick J. A., Courteau S., Faber S. M., Burstein D., Dekel A., Strauss M. A., 1997, ApJS, 109, 333
Yin J., Hou J. L., Prantzos N., Boissier S., Chang R. X., Shen S. Y., Zhang B., 2009a, A&A, 505, 497
Yin J., Hou J. L., Prantzos N., Boissier S., Chang R. X., Shen S. Y., Zhang B., 2009b, A&A, 505, 497
Zheng Z., Flynn C., Gould A., Bahcall J. N., Salim S., 2001, ApJ, 555, 393